43rd AIAA Aerospace Sciences Meeting and Exhibit, 10-13 Jan 2005, Reno, NV

LES of a Non-Premixed Flame Using an Extended Flamelet/Progress Variable Model

Matthias Ihme* and Heinz Pitsch†

Mechanical Engineering, Stanford University, Stanford, CA 94305

In previous a priori studies we have examined the flamelet/progress variable model proposed by Pierce and Moin and identified the most important areas for model improvements. The flamelet/progress variable approach is a conserved scalar based model for non-premixed combustion and uses a reactive scalar as an additional parameter in a table lookup. One of the main assumptions in this model is the use of a delta function as a presumed probability density function (PDF) for this reactive scalar. We have previously shown that the use of the beta function provides some improvement. Here, the statistically most-likely distribution is proposed as a presumed PDF for the flamelet parameter. This provides two advantages. First of all, the function depends on a chemical time-scale, and in addition, an arbitrary number of moments can be enforced. The model is applied to flames D and E of the Sandia piloted turbulent jet flame series and results are compared with experimental data.

Nomenclature

$Q(\Phi)$	*A priori* probability density function of Φ
$\widetilde{P}(\Phi)$	Probability density function of Φ
$\boldsymbol{u}$	Velocity vector
$\boldsymbol{x}$	Position
c	Progress variable
G	Filter kernel
L	Flame length
p	Pressure
t	Time
y	Species mass fraction
z	Mixture fraction

Subscripts

ref	Reference scale
SML	Statistically most-likely distribution
st	Stoichiometric condition

Symbols

α	Diffusivity
χ	Scalar dissipation rate
Δ	LES filter size
γ	Time scale ratio

*Research Assistant

†Assistant Professor

μ	Viscosity
Φ	Independent sample space variable
ϕ	Dependent stochastic variable
ρ	Density
τ	Time scale
$\boldsymbol{\tau}$	Stress tensor
θ	Temperature
$\widetilde{\phi''^2}$	Subgrid-scale variance
$\widetilde{\phi}$	Filtered or mean value
$\widetilde{\phi''^2}_<$	Resolved variance
$\boldsymbol{\sigma}$	Viscous stress tensor
ω	Chemical source term
Re	Reynolds number

I. Introduction

In recent years, large-eddy simulation (LES) has been shown to have advantages in modeling turbulent combustion processes of engineering interest. For the prediction of non-premixed turbulent combustion, the most frequently used models are flamelet models, the transported probability density function (TPDF) method,[1,2] and the conditional moment closure (CMC) method.[3,4] The Sandia flame series, including experiments on several piloted partially premixed methane/air jets at varying Reynolds numbers, has been established as one of the most important validation data bases for non-premixed combustion. In the context of Reynolds averaged (RANS) simulations, both the CMC and the TPDF model have been applied to Sandia flames D, E, and F, which increase in the extent of local extinction in that order. Pitsch and Steiner[5] and Pitsch[6] have developed an unsteady flamelet model for LES that accounts for transient effects. Applications of the model to Sandia flame D demonstrate substantially improved predictions compared with steady flamelet models. The CMC and flamelet-based models are conserved scalar based methods, and use a presumed PDF approach to describe the mixture fraction distribution. Although the application of flamelet based models to combustion with local extinction has been discussed in a priori studies,[7,8] *a posteriori* simulations have not yet been performed.

In flamelet models, typically the scalar dissipation rate appears as a parameter in addition to the mixture fraction. In the flamelet/progress variable (FPV) model recently proposed by Pierce and Moin,[9,10] all chemical quantities are expressed in terms of the mixture fraction z and a reactive scalar, such as the progress variable c or a flamelet parameter λ. In this, the model is similar to the models by Janicka & Kollmann,[11] Bruel *et al.*,[12] and Zhang *et al.*[13] where similar ideas have been used in the context of RANS. The important difference between c and λ at this juncture is that while the progress variable is still a function of z, the flamelet parameter is defined in such a way that it is truly independent of z and can therefore be thought of as a unique identifier of each single flamelet along the S-shaped curve. Here we define λ as $\lambda \equiv c(Z_{\rm st}, \chi_{\rm st})$. For the evaluation of the mean scalars, the joint PDF of the mixture fraction and the flamelet parameter $\widetilde{P}(Z,\Lambda)$ then needs to be modeled. Here, the uppercase symbols are the sample space variables of the corresponding lower case symbols. Assuming statistical independence between z and λ, the joint PDF $\widetilde{P}(Z,\Lambda)$ is modeled by using a beta distribution for the mixture fraction[14,15,16] and a delta distribution for Λ. This model has recently been applied in the context of LES by Pierce & Moin.[9,10] The key modeling assumptions of the FPV model have been assessed in an *a priori* study with particular emphasis on the prediction of extinction and re-ignition effects.[17] In this study, it was concluded that the commonly presumed delta distribution for the marginal PDF of the flamelet parameter leads to an over-prediction of the temperature. Specifically, the broad flamelet distribution caused during the highly dynamic phase of extinction and re-ignition is not accounted for using this distribution. A presumed beta distribution for the marginal PDF of λ is shown to considerably improve the results. Furthermore, it is shown that the strong assumption of statistical independence between Z and Λ, especially for regions away from the stoichiometric mixture fraction $Z_{\rm st}$, is not fully justified. This can mainly be attributed to the unsteadiness and it is argued that an unsteady FPV model further improves the results.

The present paper addresses the former issue of the modeling of the marginal PDF of Λ in an *a posteriori* sense. Here, $\widetilde{P}(\Lambda)$ is modeled by a statistically most-likely distribution and its shape is constrained by

enforcing the first and second moment of the progress variable. Additionally, a model for the residual or subgrid-scale variance of the progress variable appearing in the model formulation is presented. This extended FPV model is applied in numerical simulations of the Sandia flames D and E and the results are compared with experimental data.

The paper is organized as follows. In section II, the governing equations solved in the large-eddy simulation are presented and the FPV model and extended FPV model are described in detail. In section III, the experimental configuration used in the present simulation and the numerical setup is explained. Results, obtained with the extended FPV model are presented in section IV. The paper finishes with conclusions.

II. Mathematical Formulation

A. Governing Equations for Large-Eddy Simulation

If a Favre-filtered quantities of $\boldsymbol{\phi}$ are defined as

$$\widetilde{\boldsymbol{\phi}}(\boldsymbol{x}) = \frac{1}{\overline{\rho}} \int_\Omega \rho(\boldsymbol{x}')\boldsymbol{\phi}(\boldsymbol{x}')G(\boldsymbol{x},\boldsymbol{x}')\mathrm{d}\boldsymbol{x}' \,, \tag{1}$$

where $\overline{\rho}\widetilde{\boldsymbol{\phi}} = \overline{\rho\boldsymbol{\phi}}$, the filtered equations for mass, momentum, mixture fraction, and a progress variable can be written in non-dimensional from as

$$\begin{aligned}
\partial_t\overline{\rho} + \nabla\cdot(\overline{\rho}\widetilde{\boldsymbol{u}}) &= 0 \,, && (2a)\\
\partial_t(\overline{\rho}\widetilde{\boldsymbol{u}}) + \nabla\cdot(\overline{\rho}\widetilde{\boldsymbol{u}}\widetilde{\boldsymbol{u}}) &= -\nabla\overline{p} + \nabla\cdot\widetilde{\boldsymbol{\sigma}} + \nabla\cdot\widetilde{\boldsymbol{\tau}}_{\boldsymbol{u}}^{\mathrm{SGS}} \,, && (2b)\\
\partial_t(\overline{\rho}\widetilde{z}) + \nabla\cdot(\overline{\rho}\widetilde{\boldsymbol{u}}\widetilde{z}) &= \nabla\cdot(\overline{\rho}\alpha_z\nabla\widetilde{z}) + \nabla\cdot\widetilde{\boldsymbol{\tau}}_z^{\mathrm{SGS}} \,, && (2c)\\
\partial_t(\overline{\rho}\widetilde{c}) + \nabla\cdot(\overline{\rho}\widetilde{\boldsymbol{u}}\widetilde{c}) &= \nabla\cdot(\overline{\rho}\alpha_c\nabla\widetilde{c}) + \nabla\cdot\widetilde{\boldsymbol{\tau}}_c^{\mathrm{SGS}} + \overline{\rho}\widetilde{\omega}_c \,. && (2d)
\end{aligned}$$

Here, $\widetilde{\boldsymbol{\sigma}} = \mu\left[(\nabla\widetilde{\boldsymbol{u}}) + (\nabla\widetilde{\boldsymbol{u}})^{\intercal} - \frac{2}{3}\boldsymbol{I}\widetilde{\boldsymbol{u}}\right]$, $\widetilde{\boldsymbol{\tau}}_\phi^{\mathrm{SGS}} = \overline{\rho}(\widetilde{\boldsymbol{u}}\widetilde{\phi} - \widetilde{\boldsymbol{u}\phi})$, and the reference diameter, jet bulk velocity, and density have been used for non-dimensionalization:

$$\begin{aligned}
\rho &= \frac{\rho^*}{\rho_{\mathrm{ref}}} \,, & \boldsymbol{u} &= \frac{\boldsymbol{u}^*}{U_{\mathrm{ref}}} \,, & \nabla &= D_{\mathrm{ref}}\nabla^* \,,\\
t &= \frac{t^*U_{\mathrm{ref}}}{D_{\mathrm{ref}}} \,, & p &= \frac{p^*}{\rho_{\mathrm{ref}}U_{\mathrm{ref}}^2} \,, & c &= \frac{c^*}{C_{\mathrm{ref}}} \,,\\
\omega_c &= \frac{\omega_c^*D_{\mathrm{ref}}}{U_{\mathrm{ref}}C_{\mathrm{ref}}} \,, & \alpha_\phi &= \frac{\alpha_\phi^*}{\rho_{\mathrm{ref}}U_{\mathrm{ref}}D_{\mathrm{ref}}} \,, & \mu &= \frac{\mu^*}{\rho_{\mathrm{ref}}U_{\mathrm{ref}}D_{\mathrm{ref}}} \,.
\end{aligned} \tag{3}$$

The residual stresses $\widetilde{\boldsymbol{\tau}}_{\boldsymbol{u}}^{\mathrm{SGS}}, \widetilde{\boldsymbol{\tau}}_z^{\mathrm{SGS}}$, and $\widetilde{\boldsymbol{\tau}}_c^{\mathrm{SGS}}$ appearing in Eqs. (2) are modeled using the dynamic procedure.[18,19]

B. Combustion Model

1. *Extended Flamelet/Progress Variable Model*

In the flamelet/progress variable approach all thermodynamic and chemical quantities are specified in terms of two parameters: the mixture fraction z, which is a passive scalar, and a suitable flamelet parameter λ, which is expressed in terms of a progress variable c. Note, in the following we will use upper case letters to indicate the independent sample space variable Φ and lower case letters for the corresponding dependent stochastic variable $\phi(t,\boldsymbol{x})$. In addition to the solution of the conservation equations for mass and momentum, two additional equations $(2c)$ and $(2d)$ for z and c need to be solved in a simulation. An unclosed chemical source term $\overline{\rho}\widetilde{\omega}_c$ appears in the transport equation for $\widetilde{c}$ along with an unclosed term describing the scalar flux $\overline{\rho}\widetilde{\boldsymbol{u}c}$. In the present model, the closure of $\widetilde{\omega}_c$ is obtained by employing a presumed joint probability density function approach, which can be written as

$$\widetilde{P}(Z,\Lambda) = \widetilde{P}(Z)\widetilde{P}(\Lambda|Z) \tag{4}$$

and

$$\widetilde{\boldsymbol{\phi}} = \int_\Lambda\int_Z \boldsymbol{\phi}(Z,\Lambda)\widetilde{P}(Z,\Lambda)\mathrm{d}Z\mathrm{d}\Lambda \,, \tag{5}$$

where $\boldsymbol{\phi}(Z,\Lambda)$ is obtained from the solution of the steady laminar flamelet equations.[20] It has been shown by several authors that the PDF of a passive scalar can reasonably be approximated by a beta distribution.[14,15,16] It is well-known that the PDF of a reactive scalar cannot usually be represented by a presumed distribution, as its often multi-modal shape strongly depends on the turbulence-chemistry interaction manifested by extinction and re-ignition processes, reaction time scales, accessed regions in composition space, and higher-moment information. Often employed approximations for $\widetilde{P}(\Lambda|Z)$ or $\widetilde{P}(\Lambda)$ include (double) delta functions, (clipped) Gaussian functions, and the beta distribution. It has been shown in an *a priori* study that a presumed beta distribution for the reactive scalar results in a significant improvement of mean temperature results when compared with results obtained using a delta function, especially in the case of strong local extinction and re-ignition.[17]

In this study we will assume statistical independence between z and λ, and use the statistically most-likely distribution (SMLD) as a presumed PDF for $\widetilde{P}(\Lambda)$. The key idea of SMLD is to approximate the true PDF, which can be constructed from the knowledge of all higher moments, from a reduced set of i known higher moments, subject to the constraint that the resulting PDF, $\widetilde{P}_{\mathrm{SML},i}$, contains a minimum of information, or in other words, a maximum amount of entropy.[21]

A measure of the uncertainty of the possible states of a stochastic variable can be defined as[22,23,24,25,26]

$$H(\widetilde{P}(\Psi)) = -\int_{\Psi} \widetilde{P}(\Psi) \ln\left(\frac{\widetilde{P}(\Psi)}{Q(\Psi)}\right) d\Psi \;, \tag{6}$$

where $Q(\Psi)$ is an *a priori* PDF of the sample space variable Ψ.[26] For a passive scalar $Q(\Psi) = q$ is constant.

The *a priori* PDF $Q(\Psi)$ of a reactive scalar accounts for the bias in composition space:[26] The probability of finding a state in the composition space is inversely proportional to its composition speed due to (a) molecular mixing $v_{\mathrm{m}} = \psi'/\tau_\psi = \widetilde{\chi}_\psi/\psi'$ and (b) chemical reaction $v_{\mathrm{r}} = \omega_\psi$. Whereas large values of $Q(\Psi)$ lead to bias towards these values of Ψ, small values for $Q(\Psi)$ reduce the probability of finding a possible state. A suggested form[26,27,28] reads as

$$Q(\Psi) = \frac{1}{\psi'} \left|\left| \frac{v_{\mathrm{m}}}{v_{\mathrm{m}} + v_{\mathrm{r}}} \right|\right| \;, \tag{7}$$

where $\psi' = \sqrt{\widetilde{\psi''^2}}$ and the norm $||\cdot||$ has been introduced to guarantee that the *a priori* PDF is a positive quantity. Using calculus of variation, the PDF which maximizes the enthalpy H is found to have the form

$$\widetilde{P}_{\mathrm{SML},i}(\Psi) = Q(\Psi) \exp\left\{ \sum_i a_i \Psi^i \right\} \;, \tag{8}$$

and the subscript i denotes the number of enforced central moments and the free parameter vector $\boldsymbol{a}$ is determined subject to the constraints

$$\int_{\Psi} \widetilde{P}_{\mathrm{SML},i}(\Psi) d\Psi - 1 = 0 \;, \tag{9a}$$

$$\int_{\Psi} \Psi \widetilde{P}_{\mathrm{SML},i}(\Psi) d\Psi - \widetilde{\psi} = 0 \;, \tag{9b}$$

$$\int_{\Psi} (\Psi - \widetilde{\psi})^j \widetilde{P}_{\mathrm{SML},i}(\Psi) d\Psi - \widetilde{\psi''^j} = 0 \qquad \text{for } j = 2,\ldots,i \;. \tag{9c}$$

This can formally be written in matrix form as

$$\boldsymbol{P}(\boldsymbol{a}) = \boldsymbol{0} \tag{10}$$

and can iteratively be solved to find the roots. In the present study, Bryden's method has been used in order to find the solution vector $\boldsymbol{a}$.[29]

By employing the key model assumption that $\boldsymbol{\phi} = \boldsymbol{\phi}(z,\lambda)$ and the statistical independence between z

and λ, the constraints in (9) can solely be expressed in terms of the progress variable C

$$\int_\Lambda \left\{ \int_Z \beta(Z;\widetilde{z},\widetilde{z''^2})\mathrm{d}Z \right\} \widetilde{P}_{\mathrm{SML},i}(\Lambda;\widetilde{\lambda},\ldots,\widetilde{\lambda''^i})\mathrm{d}\Lambda - 1 = 0\,, \tag{11a}$$

$$\int_\Lambda \left\{ \int_Z C(Z,\Lambda)\beta(Z;\widetilde{z},\widetilde{z''^2})\mathrm{d}Z \right\} \widetilde{P}_{\mathrm{SML},i}(\Lambda;\widetilde{\lambda},\ldots,\widetilde{\lambda''^i})\mathrm{d}\Lambda - \widetilde{c} = 0\,, \tag{11b}$$

$$\int_\Lambda \left\{ \int_Z [C(Z,\Lambda)-\widetilde{c}]^j\, \beta(Z;\widetilde{z},\widetilde{z''^2})\mathrm{d}Z \right\} \widetilde{P}_{\mathrm{SML},i}(\Lambda;\widetilde{\lambda},\ldots,\widetilde{\lambda''^i})\mathrm{d}\Lambda - \widetilde{c''^j} = 0 \quad \text{for } j=2,\ldots,i \tag{11c}$$

and $\beta(Z;\widetilde{z},\widetilde{z''^2})$ is the well-known beta distribution, parameterized by the first two moments. The *a priori* PDF appearing in Eq. (8) can be written as

$$Q(\Lambda) = \frac{1}{\sqrt{\widetilde{c''^2}}} \left[1 + \left(\frac{\omega_c(Z_{\mathrm{st}},\Lambda)}{\chi_z(Z_{\mathrm{st}},\Lambda)} \frac{\gamma\widetilde{z''^2}}{\sqrt{\widetilde{c''^2}}} \right)^2 \right]^{-1/2} . \tag{12}$$

where the time-scale ratio

$$\gamma = \frac{\tau_c}{\tau_z} = \frac{\widetilde{c''^2}}{\widetilde{z''^2}} \frac{\widetilde{\chi}_z}{\widetilde{\chi}_c} \tag{13}$$

has been used to replace the unknown dissipation rate of the progress variable, $\widetilde{\chi}_c$. The chemical source term and scalar dissipation rate are evaluated at the stoichiometric mixture fraction, Z_{st}.

2. Model for the Subgrid-Scale Variance for Conserved and Reactive Scalar

The subgrid-scale variance of the mixture fraction, $\widetilde{z''^2}$, is modeled by assuming that the rate of production and dissipation are in equilibrium[19]

$$\widetilde{z''^2} = \mathcal{C}_z \Delta^2 |\nabla\widetilde{z}|^2 \tag{14}$$

and $\mathcal{C}_z$ is computed by a dynamic procedure.

Similarly, the subgrid-scale variance of the progress variable is modeled assuming that production, dissipation and the progress variable-chemical source term correlation in the subgrid-scale variance transport equation are in equilibrium:

$$2\widetilde{\boldsymbol{u}''c''}\cdot\nabla\widetilde{c} + \widetilde{\chi_c''} = 2\widetilde{c''\omega_c''}\,, \tag{15}$$

where $\widetilde{\chi}_\phi = \widetilde{\chi}_\phi^{\mathrm{res}} + \widetilde{\chi_\phi''} = 2\alpha_\phi|\nabla\widetilde{\phi}|^2 + 2\alpha_\phi\widetilde{|\nabla\phi''|^2}$. The scalar flux term is modeled by a gradient diffusion model, $\widetilde{\boldsymbol{u}''c''} = -\alpha_{t,c}\nabla\widetilde{c}$, and the turbulent diffusivity $\alpha_{t.c}$ is computed from a dynamic procedure.[19] The subgrid dissipation rate of the progress variable can be expressed by $\widetilde{z''^2}$ and $\widetilde{\chi}_z$ using Eq. (13) which results in the model for the subgrid-scale progress variable

$$\widetilde{c''^2} = \frac{\gamma\widetilde{z''^2}}{\widetilde{\chi}_z} \left[2\alpha_{t,c}|\nabla\widetilde{c}|^2 + 2\widetilde{c''\omega_c''} + \widetilde{\chi}_c^{\mathrm{res}} \right] . \tag{16}$$

It is also possible to directly solve a modeled form of the transport equation for the subgrid-scale variance

$$\partial_t(\overline{\rho}\widetilde{c''^2}) + \nabla\cdot(\overline{\rho}\widetilde{\boldsymbol{u}}\widetilde{c''^2}) = \nabla\cdot(\overline{\rho}\alpha_c\nabla\widetilde{c''^2}) + \nabla\cdot\widetilde{\boldsymbol{\tau}}_c^{\mathrm{SGS}} + 2\overline{\rho}\widetilde{c''\omega_c''} - \overline{\rho}\widetilde{\chi_c''} - 2\overline{\rho}\widetilde{\boldsymbol{u}''c''}\cdot\nabla\widetilde{c}\,. \tag{17}$$

The term $\widetilde{c''\omega_c''}$ in Eq. (17) is obtained from the presumed PDF-model and $\widetilde{\chi_c''}$ can be expressed in terms of γ, $\widetilde{z''^2}$ and $\widetilde{\chi}_z$ using Eq. (13). Both models, Eqs. (16) and (17), rely on models for the subgrid-scale mixture fraction variance and scalar dissipation rate. The subgrid-scale variance of the progress variable, obtained from Eq. (17), turns out to be smoother when compared with the solution of Eq. (16), resulting in a more stable simulation. Therefore, results obtained with the second model will be presented in the following.

III. Experimental and Numerical Setup

A. Experimental Conditions

The flamelet/progress variable model is applied to the unconfined turbulent, piloted jet diffusion flames D and E of Barlow & Frank.[30,31] The central jet nozzle has a diameter of $D = 7.2$ mm and the annular pilot nozzle diameter is 18.2 mm. The oxidizer air at 291 K is supplied in a co-flow. The fuel jet velocities are 49.6 ($\pm$2) and 74.4 ($\pm$2) m/s and the pilot gas velocity is 11.4 ($\pm$0.5) and 17.1 ($\pm$0.75) m/s for flames D and E, respectively. The co-flow velocity is 0.9 ($\pm$0.05) m/s. The Reynolds numbers, based on the nozzle diameter, jet bulk exit velocity and kinematic viscosity of the fuel jet, are 22,400 and 33,600, respectively.

The jet fluid consists of a mixture of methane and air in a volumetric ratio of 1 : 3 with a stoichiometric mixture fraction of $Z_{\rm st} = 0.351$. The pilot stream is a lean premixed gas mixture of C_2H_2, H_2, CO_2, N_2, and air with an equivalence ratio of 0.77 and a similar equilibrium composition as the jet fuel with $Z_{\rm st} = 0.271$. It has been reported that these flames burn as diffusion flames and exhibit no significant premixed reaction zone in the fuel-rich region.

In the following section, ensemble averaged and conditional statistics obtained from the numerical simulation will be compared with experimental data. For clarity, the following notation is introduced:

$$\langle\widetilde{\phi}(x,r)\rangle = \frac{1}{2\pi T}\int_t^{t+T}\int_0^{2\pi}\widetilde{\phi}(t,x,r,\varphi)\mathrm{d}\varphi\mathrm{d}t\ , \tag{18a}$$

$$\langle\widetilde{\phi}''^2_<(x,r)\rangle = \frac{1}{2\pi T}\int_t^{t+T}\int_0^{2\pi}(\widetilde{\phi}(t,x,r,\varphi) - \langle\widetilde{\phi}(x,r)\rangle)^2\mathrm{d}\varphi\mathrm{d}t\ , \tag{18b}$$

where $\langle\widetilde{\phi}''^2_<\rangle$ is the resolved variance and $\widetilde{\phi}$ is obtained from Eqs. (1) or (5).

B. Numerical Simulation

The conservation equations for mass, momentum, mixture fraction, and progress variable are solved in cylindrical coordinates.[9]

The geometry has been non-dimensionalized by the jet nozzle diameter D and the computational domain is $70D \times 23.5D \times 2\pi$ in the axial, radial, and circumferential direction, respectively. The radial direction is discretized by 152 unevenly spaced grid points concentrated in the fuel and pilot stream. For the fuel jet radius and pilot annulus 18 and 33 grid points are used. The grid in axial direction uses 256 points and is stretched in downstream direction while the circumferential direction is equally spaced and uses 64 points. The minimum and maximum filter width in the domain are $\Delta_{\rm min} = 4.14 \times 10^{-2}$ (boundary layer in the fuel jet) and $\Delta_{\rm max} = 1.01$ (outermost grid cell at the outflow plane). A section of the axi-symmetric computation domain is shown in Fig. 1.

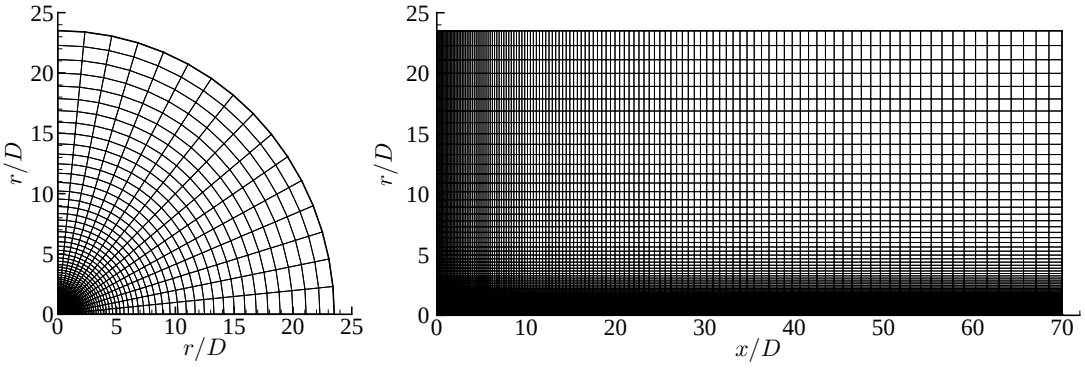

Figure 1. Numerical grid used for the large-eddy simulation. Only a section of the axi-symmetric domain and every second grid point in the axial and radial direction are shown.

The turbulent inlet velocity profile is generated by separately performing a periodic pipe flow simulation, enforcing the mean and rms axial velocity components as measured by Schneider *et al.*[32]

The numerical simulation is run over ten flow-through-times to obtain a statistically stationary flow field, and statistics are collected thereafter over 5 flow-through-times.

C. Chemistry Mechanism and Combustion Model

Steady flamelet calculations have been performed using the FLAMEMASTER code.[33] Chemistry is described by the GRI 2.11 mechanism,[34] consisting of 279 reactions among 49 species.

Pitsch[35] has argued that only a thin region around the reaction zone is governed by molecular transport, whereas the outer mixing region is dominated by turbulent transport implying unity Lewis number. Hence, the Lewis numbers of all chemical species are assumed to be unity. In the present simulation the progress variable is defined as $c \equiv y_{\mathrm{CO_2}} + y_{\mathrm{CO}} + y_{\mathrm{H_2O}} + y_{\mathrm{H_2}}$. Radiation has not been considered in the present simulation. As a result, the peak temperature in the downstream region is presumably over-predicted by about $50 - 100$ K using the present model. By introducing the enthalpy as an additional progress variable, the FPV model has been extended to incorporate thermal radiation effects. Results obtained with this model confirm that the mean centerline temperature for flame D is reduced by approximately 100 K for $x/D > 40$.

After integrating the flamelets with the presumed PDF, the mean value of all chemical quantities are a function of four parameters, $\widetilde{\boldsymbol{\phi}} = \widetilde{\boldsymbol{\phi}}(\widetilde{z}, \widetilde{z''^2}, \widetilde{c}, \widetilde{c''^2})$. The library is discretized with 100 and 75 uniformly distributed grid points in the $\widetilde{z}$ and $\widetilde{c}$ directions, respectively. For both the $\widetilde{z''^2}$ and $\widetilde{c''^2}$ directions, 20 points are used and the grid spacing follows a geometric growth law.

In the present simulation, the time scale ratio, appearing in Eqs. (12) and (17), is set to unity. In principle, a model based on the mapping closure following Cha et al.[36,37] could be employed for a better prediction of γ. This, however, would then introduce γ as a fifth independent parameter into the FPV model.

IV. Results and Discussion

A. Sandia Flame D

The axial profiles for mean and rms value of axial velocity, mixture fraction and temperature are shown in Fig. 2. The velocity is normalized by the jet bulk velocity. Results obtained with the extended FPV model (solid lines) are compared with experimental data (symbols). The velocity profiles obtained form the simulation are in reasonable agreement with experimental data from the LDV-measurements. The velocity near the nozzle, $x/D < 15$, is under-predicted and over-predicted thereafter. The potential core is virtually not existing. The reason for this cannot be attributed to insufficient grid resolution, as in the region near the nozzle, say for $x/D = 5$, the ratio of filter width to Kolmogorov length scale is roughly $\Delta/\eta \approx 7$. This is estimated from[38] $\mathrm{Re}_T \sim \frac{1}{20}\mathrm{Re}_\lambda^2$, $\sqrt{\langle \widetilde{u}_<'' \rangle}/U_J = 0.055$, and turbulent kinetic energy of $k/U_J^2 = 2.64 \times 10^{-3}$. The turbulent intensity is slightly under-predicted for $10 \leq x/D \leq 30$.

The second row in Fig. 2 shows the comparison of the predicted and measured mean and rms mixture fraction. The decay rate of the mean mixture fraction is under-predicted compared with the experimental data after $x/D > 20$ which results in an over-prediction of the stoichiometric flame length $L_{\mathrm{st}} = 53.4D$. The experimentally determined flame length is $L_{\mathrm{st}} = 48D$. The resolved rms mixture fraction is in excellent agreement with experimental data.

The axial profiles of the mean and rms temperature are shown in the bottom row of Fig. 2. The mean temperature profile is closely linked to the mixture fraction profile: the mean temperature is under-predicted in the rich part for $x < L_{\mathrm{st}}$ and over-predicted thereafter which is caused due to the slow decay of the mean mixture fraction. The over-predicted mean temperature by approximately 100 K in the far field is also attributed to the fact that the present FPV model does not account for thermal radiation effects.

Turbulent non-premixed combustion processes are strongly effected by an intense interaction between chemistry on the small scales and turbulent mixing. For an appropriate assessment of only the combustion model it is essential to separate both effects. This can be accomplished by comparing data, conditioned on the mixture fraction.

Figures 3 and 4 show the computed and measured conditional mean values for temperature and reactive scalars ($\mathrm{CH_4}, \mathrm{O_2}, \mathrm{H_2O}, \mathrm{CO_2}, \mathrm{CO}, \mathrm{H_2}, \mathrm{OH}$) for flame D at four downstream axial positions, $x/D = \{7.5, 15, 30, 45\}$. The computed temperature for all four measurement stations is in excellent agreement on

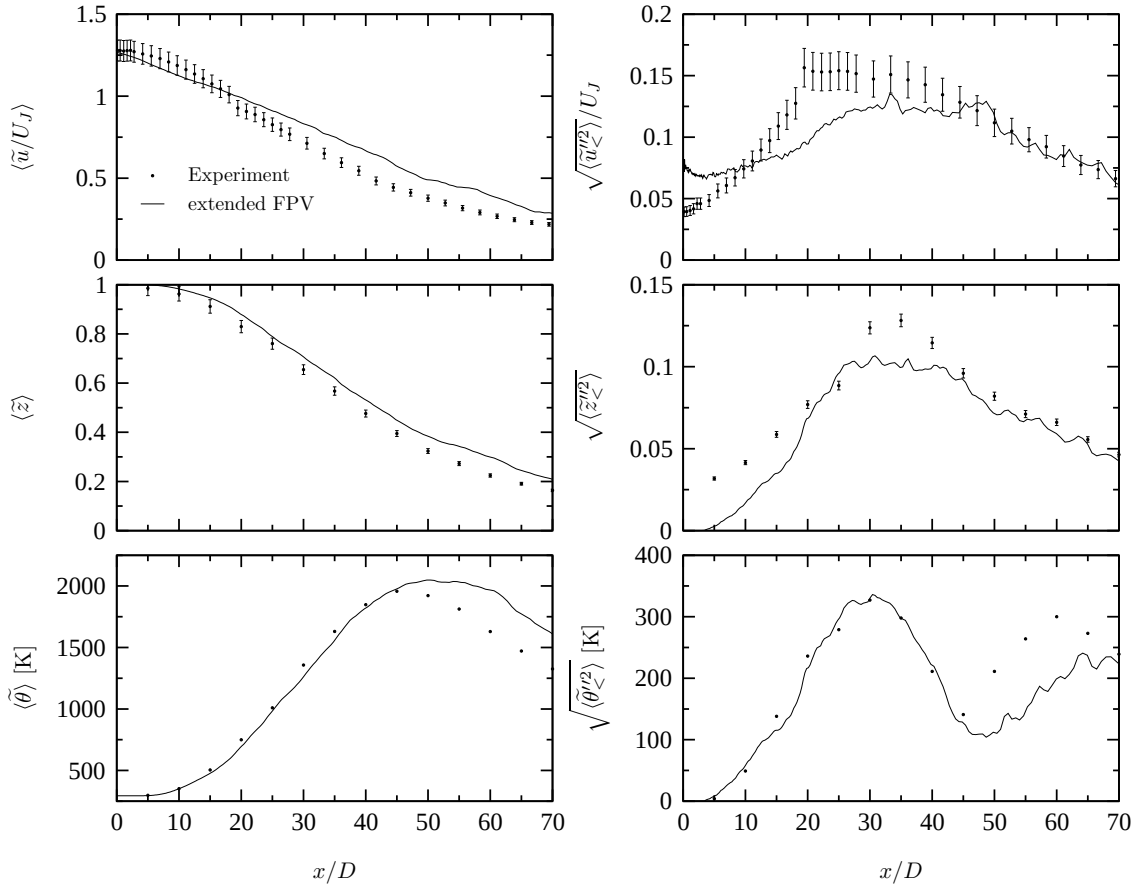

Figure 2. Comparison of measured and calculated mean and rms statistics of axial velocity, mixture fraction and temperature along the centerline for flame D. Experimental data are plotted with estimated uncertainties (symbols) and extended FPV (solid lines).

the fuel-lean side and consistently over-predicted by approximately 100 K on the rich side. A partially premixed reaction zone on the rich side is not apparent. The simulation using the FPV model predicts an higher fuel-consumption on the rich side which might be due the under-predicted local extinction for $x/D < 30$. Near the nozzle the mass fraction of molecular oxygen is under-predicted for $0.35 \leq \widetilde{z} \leq 0.5$. This and the higher methane-consumption results in the higher prediction of the major products H_2O and CO_2 for the first two measurement stations. Both, H_2O and CO_2 are in excellent agreement with experimental data for $x/D \geq 30$. The carbon in the fuel is converted to carbon monoxide, and consequently, the higher fuel consumption on the rich side results in the over-prediction of CO. CO on the lean side is in good agreement with experimental data. The peak value of the intermediate hydroxyl radical is over-predicted at the first two measurement stations, shown in Fig. 4, by approximately 30% and 18% for $x/D = 7.5$ and 15, respectively. Results for the other two downstream stations are in excellent agreement with experimental data.

B. Sandia Flame E

Flame E is characterized by a higher level of local extinction and re-ignition and is therefore a more demanding test case for combustion models. The characteristic Reynolds number, based on the jet bulk velocity, jet nozzle diameter and kinematic viscosity, is 33,600.

Mean and rms results obtained from the numerical simulation along the centerline are compared with experimental data for flame E in Fig. 5. The predicted mean velocity profile shows tendentially a similar behavior as for flame D: the velocity decay rate is under-predicted for $x/D > 20$. However, the potential core, predicted by the simulation, is slightly more pronounced as for flame D. The resolved velocity fluctuations $\sqrt{\langle\widetilde{u}''^2_<\rangle}$ is smaller than for flame D. The peak at $x/D \sim 20$ is predicted too low in the simulation. The

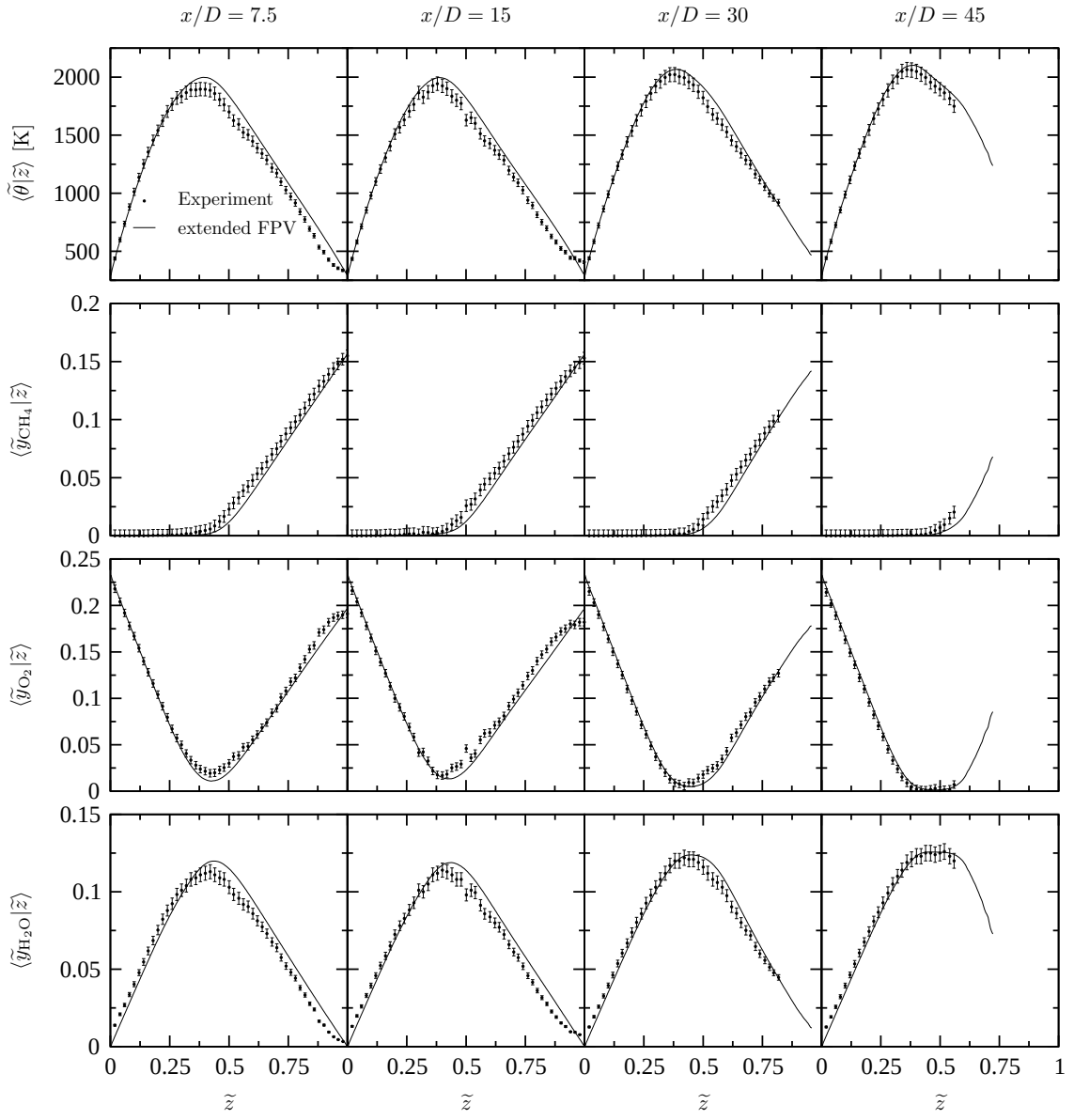

Figure 3. Comparison of measured and calculated conditional mean mass fractions of major species and temperature at $x/D = 7.5, 15, 30$ and 45 for flame D. Experimental data are plotted with estimated uncertainties (symbols) and extended FPV (solid lines).

second row in Fig. 5 shows the mean and resolved rms mixture fraction. The mean mixture fraction is over-predicted and hence the stoichiometric flame length is too long. The flame length extracted from the simulation is $L_{\rm st} = 55.5$ compared to $L_{\rm st} = 50$ from the experiment. The mean temperature, shown in the bottom row of Fig. 5, is in excellent agreement with the experiment. However, it can be anticipated that a correct prediction of the mixture fraction field will result in a higher mean temperature profile. The resolved temperature fluctuations are again in good agreement between experiment and simulation. The first peak at $x/D \sim 30$ is correctly predicted and the second peak at $x/D \sim 60$ is under-predicted.

Figure 6 and 7 shows the conditional mean quantities for temperature, major and minor species at axial position $x/D = \{7.5, 15, 30, 45\}$. The mean temperature at the first two measurement stations in Fig. 6, obtained from the simulation, is in good agreement in the lean part but is over-predicted at the fuel-rich side. A premixed reaction zone is not visible in the simulation. This good agreement between simulation and experiment is evident for $x/D = 30$ and 45, where the temperature is mainly due to post-reaction and heat diffusion. As already observed for flame D, the fuel consumption rate is slightly too high on the rich side,

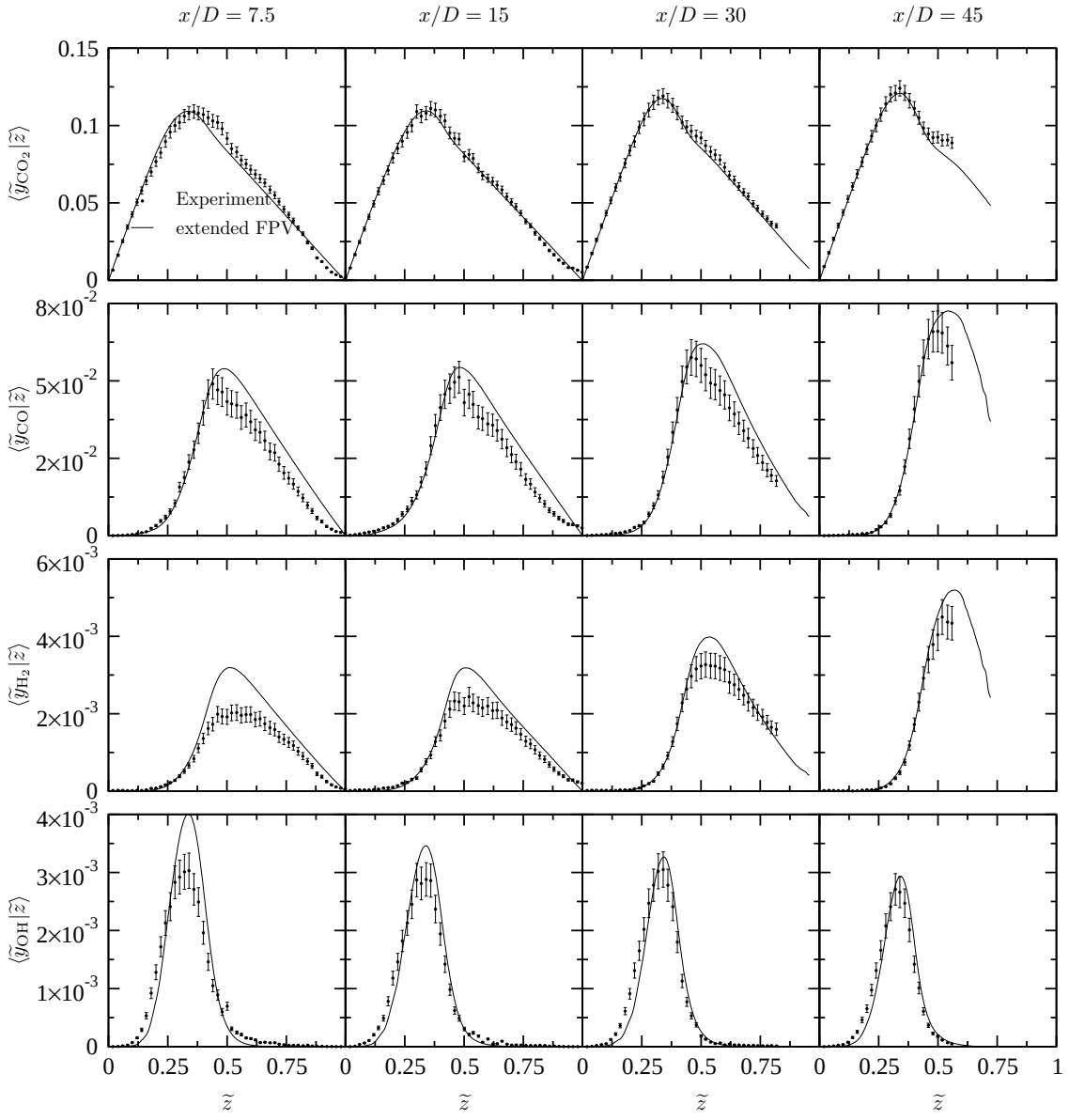

Figure 4. Comparison of measured and calculated conditional mean mass fractions of chemical species at $x/D = 7.5, 15, 30$ and 45 for flame D. Experimental data are plotted with estimated uncertainties (symbols) and extended FPV (solid lines).

compared with experimental data. This and the under-predicted O_2 mass fraction, shown in third row of Fig. 6, results in an over-prediction for the stable species CO and H_2O. Carbon dioxide, shown in Fig. 7, as major product species, is in excellent agreement with the experimental data. Considering the elevated level of extinction for flame E in the region $x/D < 30$, all major and minor product mass fractions can considered to be in good agreement with the experimental data.

V. Conclusions

The flamelet/progress variable approach of Pierce & Moin[9,10] has been extended for the prediction of local extinction and re-ignition effects in turbulent diffusion flames.

A presumed PDF, based on the statistically most-likely distribution, has been used for the marginal PDF of the flamelet parameter. The shape of this PDF is determined by enforcing the first two moments of the

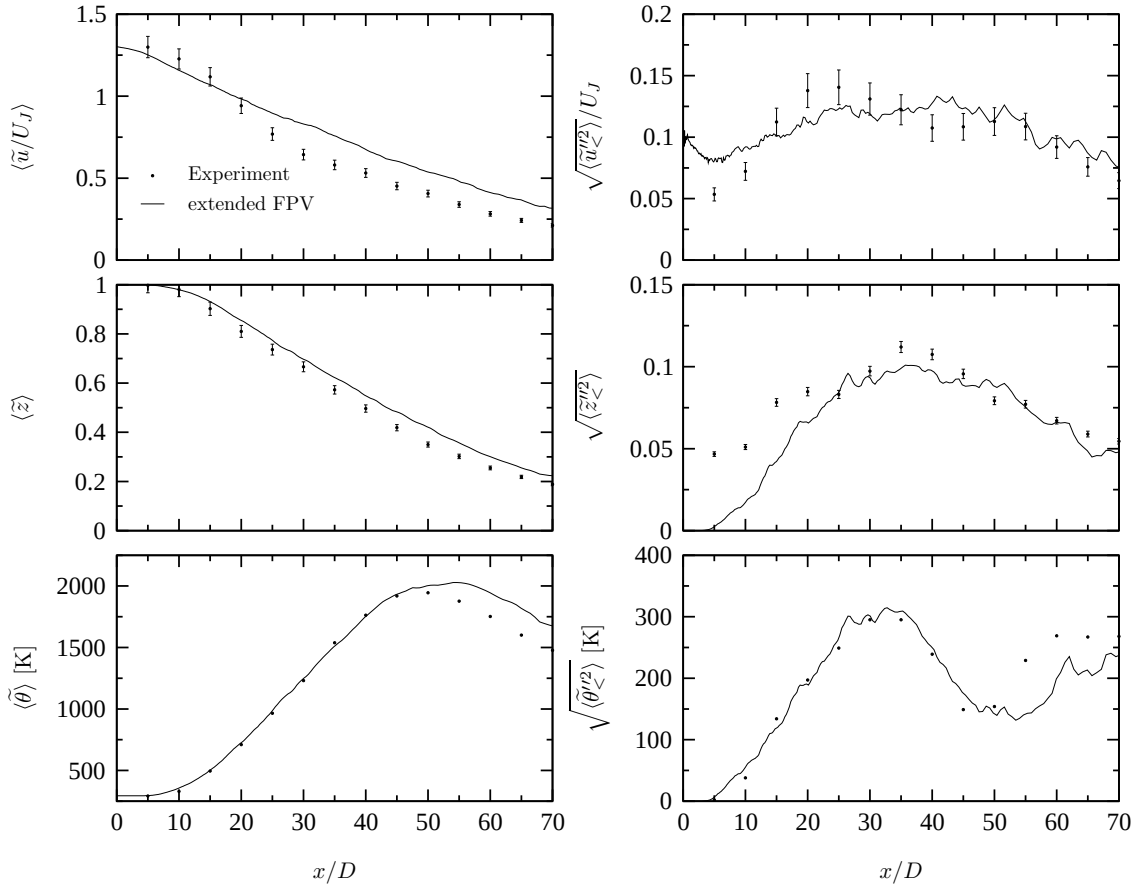

Figure 5. Comparison of measured and calculated mean and rms statistics of axial velocity, mixture fraction and temperature along the centerline for flame E. Experimental data are plotted with estimated uncertainties (symbols) and extended FPV (solid lines).

progress variable. The extended FPV model requires then, in addition to $\widetilde{z}, \widetilde{z''^2}$ and $\widetilde{c}$, the solution of the subgrid-scale progress variable variance. Two models for $\widetilde{z''^2}$ have been proposed which both introduce the time scale ratio γ. In the present paper, $\widetilde{c''^2}$ is obtained from the solution of a transport equation for $\widetilde{c^2}$.

The extended FPV model has been applied in an large-eddy simulation of Sandia flames D and E. The results obtained for both cases are in good agreement with experimental data. This demonstrates the ability of the extended FPV model to predict local extinction and re-ignition effect in turbulent diffusion flames.

Acknowledgments

The authors gratefully acknowledge funding by the US Department of Energy under the ASCI program.

References

[1]Lindstedt, R., Louloudi, S., and Vaós, E., "Joint scalar probability density function modeling of pollutant formation in piloted turbulent jet diffusion flames with comprehensive chemistry," *Proc. Combust. Inst. 28*, 2000, pp. 149–156.

[2]Xu, J. and Pope, S., "PDF calculations of turbulent nonpremixed flames with local extinction," *Combust. Flame*, Vol. 123, No. 3, 2000, pp. 281–307.

[3]Kim, S. and Huh, K., "Second-order conditional moment closure modeling of turbulent piloted jet diffusion flames," *Combust. Flame*, Vol. 138, 2004, pp. 336–352.

[4]Kim, S., Huh, K., and Bilger, R., "Second-order conditional moment closure modeling of local extinction and reignition in turbulent nonpremixed hydrocarbon flames," *Proc. Combust. Inst. 29*, 2002, pp. 141–148.

[5]Pitsch, H. and Steiner, H., "Large-eddy simulation of a turbulent piloted methane/air diffusion flame (Sandia flame D)," *Phys. Fluids*, Vol. 12, No. 10, 2000, pp. 2541–2554.

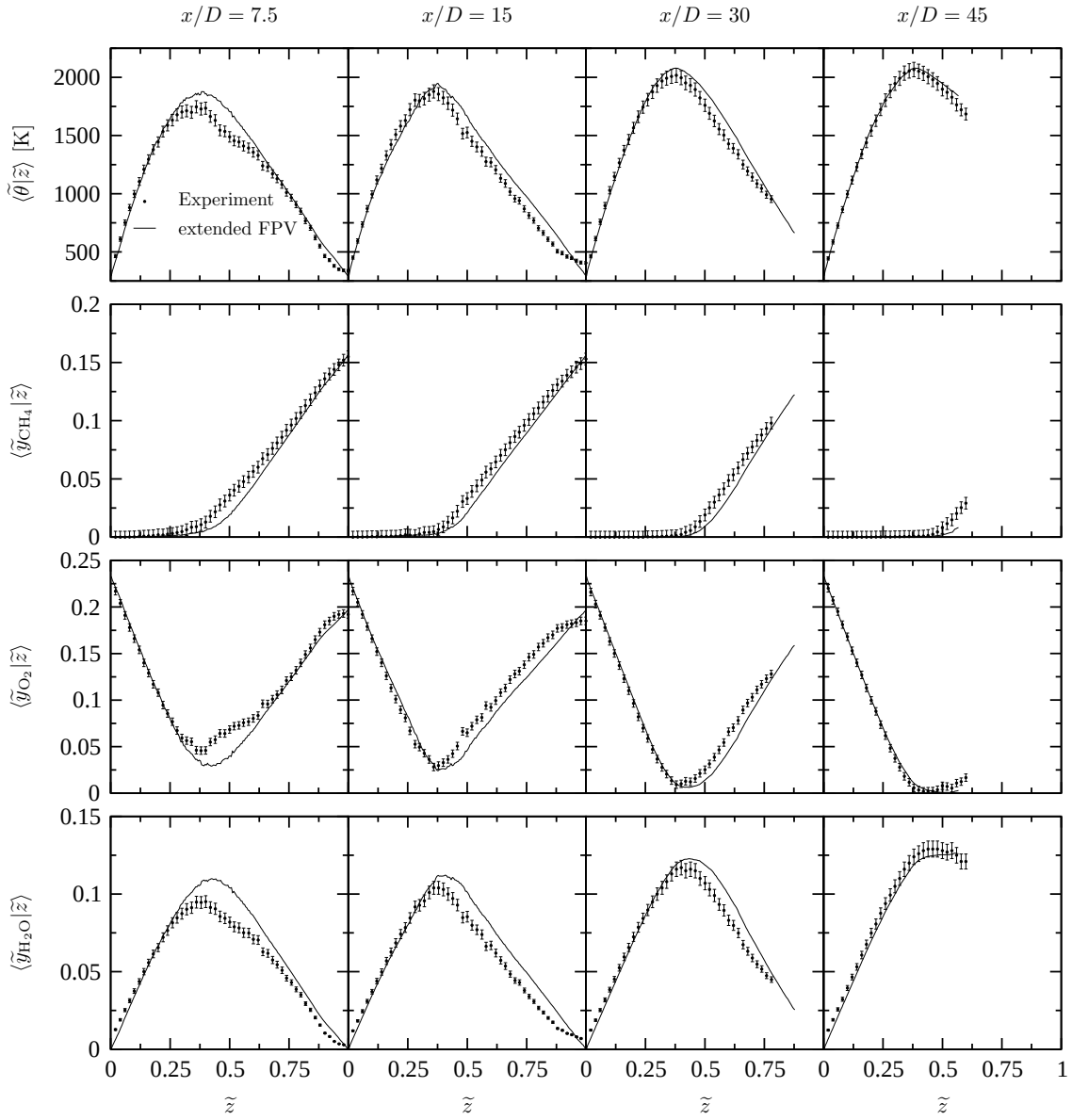

Figure 6. Comparison of measured and calculated conditional mean mass fractions of major species and temperature at $x/D = 7.5, 15, 30$ and 45 for flame E. Experimental data are plotted with estimated uncertainties (symbols) and extended FPV (solid lines).

[6]Pitsch, H., "Improved Pollutant Predictions in Large-Eddy Simulations of Turbulent Non-Premixed Combustion by Considering Scalar Dissipation Rate Fluctuations," *Proc. Combust. Inst.*, Vol. 29, 2002, pp. 1971–1978.

[7]Pitsch, H., Cha, C. M., and Fedotov, S., "Flamelet modelling of non-premixed turbulent combustion with local extinction and re-ignition," *Comb. Theory Modelling*, Vol. 7, 2003, pp. 317–332.

[8]Sripakagorn, P., Mitarai, S., Kosály, G., and Pitsch, H., "Extinction and Reignition in a Diffusion Flame (A direct numerical study)," *J. Fluid Mech.*, Vol. 518, 2004, pp. 231–259.

[9]Pierce, C. and Moin, P., "Progress-variable approach for large eddy simulation of turbulent combustion," Report No. TF-80, Stanford University, 2001.

[10]Pierce, C. and Moin, P., "Progress-variable approach for large-eddy simulation of non-premixed turbulent combustion," *J. Fluid Mech.*, Vol. 504, 2004, pp. 73–97.

[11]Janicka, J. and Kollmann, W., "A two-variable formalism for the treatment of chemical reactions in turbulent H_2-air diffusion flames," *Proc. Combust. Inst. 17*, 1978, pp. 421–430.

[12]Bruel, P., Rogg, B., and Bray, K., "On auto-ignition in laminar and turbulent non-premixed systems," *Proc. Combust. Inst. 23*, 1990, pp. 759–766.

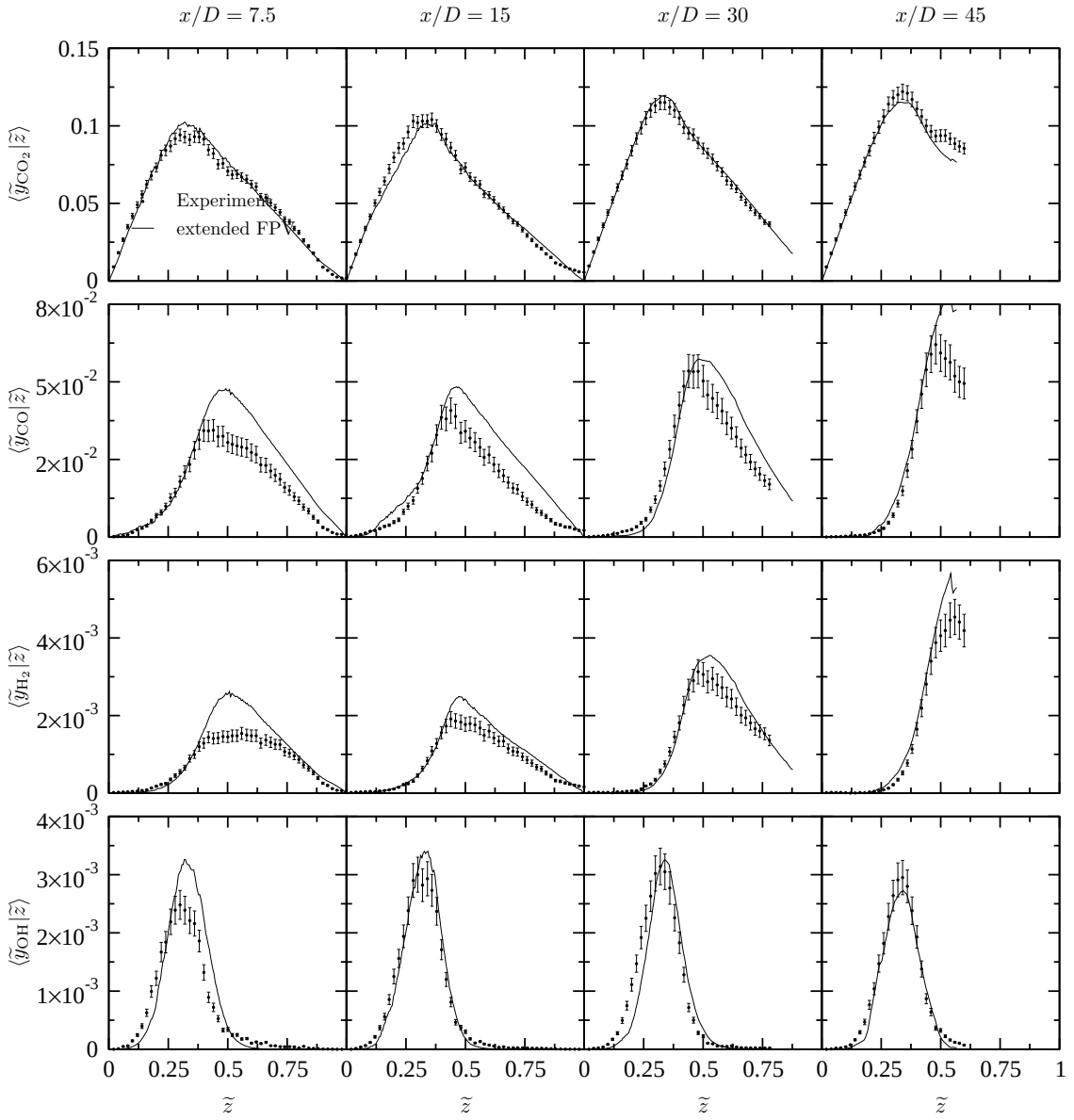

Figure 7. Comparison of measured and calculated conditional mean mass fractions of chemical species at $x/D = 7.5, 15, 30$ and 45 for flame E. Experimental data are plotted with estimated uncertainties (symbols) and extended FPV (solid lines).

[13]Zhang, Y., Rogg, B., and Bray, K., "2-D simulation of turbulent autoignition with transient laminar flamelet source term closure," *Combust. Sci. and Tech.*, Vol. 105, 1995, pp. 211–227.

[14]Cook, A. and Riley, J., "A subgrid model for equilibrium chemistry in turbulent flows," *Phys. Fluids*, Vol. 6, No. 8, 1994, pp. 2868–2870.

[15]Jiménez, J., Linãń, A., Rogers, M., and Higuera, F., "A priori testing of subgrid models for chemically reacting nonpremixed turbulent shear flows," *J. Fluid Mech.*, Vol. 349, 1997, pp. 149–171.

[16]Wall, C., Boersma, B., and Moin, P., "An evaluation of the assumed beta probability density function subgrid-scale model for large eddy simulation of nonpremixed, turbulent combustion with heat release," *Phys. Fluids*, Vol. 12, No. 10, 2000, pp. 2522–2529.

[17]Ihme, M., Cha, C., and Pitsch, H., "Prediction of local extinction and re-ignition effects in non-premixed turbulent combustion using a flamelet/progress variable approach," *Proc. Combust. Inst. 30*, 2004, pp. 793–800.

[18]Moin, P., Squires, K., Cabot, W., and Lee, S., "A dynamic subgrid-scale model for compressible turbulence and scalar transport," *Phys. Fluids*, Vol. 3, No. 11, 1991, pp. 2746–2757.

[19]Pierce, C. and Moin, P., "A dynamic model for subgrid-scale variance and dissipation rate of a conserved scalar," *Phys. Fluids*, Vol. 10, No. 12, 1998, pp. 3041–3044.

[20]Peters, N., *Turbulent Combustion*, Cambridge University Press, Cambridge, 2000.

[21]Heinz, S., *Statistical Mechanics of Turbulent Flows*, Springer-Verlag, Berlin, 2003.

[22]Shannon, C., "A mathematical theory of communication," *Bell System Tech. J.*, Vol. 27, No. 3, 1948, pp. 379–423.

[23]Jaynes, E., "Information theory and statistical mechanics," *Phys. Rev.*, Vol. 106, No. 4, 1957, pp. 620–630.

[24]Rumsey, H. and Posner, E., "Joint distributions with prescribed moments," *Ann. Math. Statist.*, Vol. 36, No. 1, 1965, pp. 286–298.

[25]Good, I., "Maximum-entropy for hypothesis formulation, especially for multidimensional contingency-tables," *Ann. Math. Statist.*, Vol. 34, No. 3, 1963, pp. 911–934.

[26]Pope, S., "A rational method of determining probability distributions in turbulent reacting flows," *J. Non-Equilib. Thermodyn.*, Vol. 4, 1979, pp. 309–320.

[27]Pope, S., "The statistical theory of turbulent flames," *Phil. Trans. Roy. Soc. London*, Vol. 291, No. 1384, 1979, pp. 529–568.

[28]Pope, S., "Probability distributions of scalars in turbulent shear flow," *Turbulent Shear Flows*, edited by J. Bradbury, F. Durst, F. Schmidt, and J. Whitelaw, Vol. 2, Springer–Verlag, Berlin, 1980, pp. 7–16.

[29]Press, W., Teukolsky, S., Vetterling, W., and Flannery, B., *Numerical Recipes in C : The Art of Scientific Computing*, Cambridge University Press, Cambridge, 1992.

[30]Barlow, R. and Franks, J., "Effects of turbulence on species mass fractions in methane/air jet flames," *Proc. Combust. Inst. 27*, 1998, pp. 1087–1095.

[31]International Workshop on Measurement and Computation of Turbulent Nonpremixed Flames, `http://www.ca.sandia.gov/TNF/`.

[32]Schneider, C., Dreizler, A., Janicka, J., and Hassel, E., "Flow field measurements of stable and locally extinguishing hydrocarbon-fuelled jet flames," *Combust. Flame*, Vol. 135, No. 1-2, 2003, pp. 185–190.

[33]Pitsch, H., "FlameMaster v3.1: a C++ computer program for 0D combustion and 1D laminar flame calculations," available from `http://www.stanford.edu/~hpitsch/`.

[34]Bowman, C., Hanson, R., Davidson, D., Gardiner, W. J., Lissianski, V., Smith, G., Golden, D., Frenklach, M., and Goldenberg, M., "GRI-Mech 2.11," available from `http://www.me.berkeley.edu/gri-mech/`.

[35]Pitsch, H., "Unsteady flamelet modeling of differential diffusion in turbulent jet diffusion flames," *Combust. Flame*, Vol. 123, No. 3, 2000, pp. 358–374.

[36]Cha, C. M. and Trouillet, P., "A model for the mixing time scale of a turbulent reacting scalar," *Phys. Fluids*, Vol. 15, No. 6, 2003, pp. 1375–1380.

[37]Cha, C. M. and Trouillet, P., "A subgrid-scale mixing model for large-eddy simulations of turbulent reacting flows using the filtered density function," *Phys. Fluids*, Vol. 15, No. 6, 2003, pp. 1496–1504.

[38]Pope, S., *Turbulent Flows*, Cambridge University Press, Cambridge, 2000.